MISARA: Matlab Interface for Seismo-Acoustic aRray Analyss

Minio, V.[1], Zuccarello[2,3], L., De Angelis[2,3], S., Di Grazia, G.[4], Saccorotti, G.[3]

[1]Dipartimento di Scienze Biologiche, Geologiche ed Ambientali - Sezione di Scienze della Terra, Università degli Studi di Catania, Catania, Italy.

[2]School of Environmental Sciences, University of Liverpool, Liverpool, UK.

[3]Istituto Nazionale di Geofisica e Vulcanologia, Sezione di Pisa, Pisa, Italy.

[4]Istituto Nazionale di Geofisica e Vulcanologia, Sezione di Catania-Osservatorio Etneo, Catania, Italy.

Corresponding authors: Vittorio Minio (vittorio.minio@phd.unict.it), Luciano Zuccarello (luciano.zuccarello@ingv.it)

ABSTRACT

Volcanic activity produces a broad spectrum of seismic and acoustic signals, whose characteristics often provide important clues on the underlying magmatic processes. Seismic and acoustic networks and arrays are the backbone of many modern volcano monitoring programmes. The investigation of the signals gathered by these instruments requires ad-hoc data analysis techniques. Continuous monitoring of the seismo-acoustic signals recorded by multi-station networks with high sampling rate leads to rapid accumulation of large volumes of data, making the implementation of fast and automated workflows for the extraction of monitoring parameters a crucial task for effective volcano surveillance. Here, we present an open-source Matlab GUI (Graphical User Interface), MISARA (Matlab Interface for Seismo-Acoustic aRray Analysis), designed to provide an efficient and user-friendly workflow for the analysis of seismo-acoustic data in volcanic environments. MISARA includes efficient algorithm implementations of well-established techniques of data analysis. It is designed to support visualization, characterization, detection and localization of volcano seismo-acoustic signals. Its intuitive, modular, structure facilitates rapid, semi-automated, inspection of data and results, thus reducing user effort. MISARA was tested using seismic data recorded at Etna Volcano (Italy) in 2010 and 2011 and is intended for use in education and research, and to support routine data analysis at volcano observatories.

INTRODUCTION

Volcano seismology deals with a large variety of seismic and acoustic signals (e.g., McNutt et al., 2015). Monitoring these waveforms plays a key role in the surveillance of volcanoes and has the potential to provide important insights on magmatic and hydrothermal processes in the plumbing system of a volcano (e.g., Sparks et al., 2012; Chouet and Matoza, 2013; McNutt et al., 2015). One of the major challenges is the investigation of the wavefield properties of these signals, in particular their source location. The application of traditional travel-time inversion methods to data from sparse networks, in particular when dealing with emergent or sustained signals such as Long Period (LP) or Very Long Period (VLP) events and volcanic tremor, is challenging. Due to the nature of these signals, other localization methods have been used in recent years including amplitude-based techniques (Di Grazia et al., 2006; Carbone et al., 2008; Cannata et al., 2013; Morioka et al., 2017) and array methods (e.g., Rost and Thomas, 2002).

Seismic and acoustic arrays consist of multiple sensors arranged according to a spatial scale significantly shorter than the wavelength of interest. In array analysis, all waveforms recorded by each sensor are processed together on the basis of the common waveform model of the signal (Aki and Richards, 1980). Depending on the specific propagation model (i.e., plane vs spherical wavefronts), the source location can be inferred directly or from back-propagation of the wave-vectors determined from the coherent wavefield propagation across the array (Havskov and Alguacil, 2016). Several studies have employed array techniques to investigate the evolution of seismic and acoustic sources during periods of volcanic unrest (Saccorotti et al., 2004; Di Lieto et al., 2007; Inza et al., 2014; Eibl et al., 2017; De Angelis et al., 2020), although their use as a monitoring tool still remains limited (e.g., Coombs et al., 2018).

Over the past decade, the amount of monitoring data from active volcanoes has grown tremendously, making the analysis of such large amounts of information a challenging task. At the same time, a plethora of software packages and algorithms for signal processing were developed in different programming environments, including the Python and Matlab platforms. Most of these packages are command-line toolboxes designed to provide a broad range of functionalities for management and handling of waveform data and related metadata, such as ObsPy (Beyreuther et al., 2010), SEIZMO (Euler, 2014) and GISMO (Thompson and Reyes., 2018). Other software toolboxes were designed with a narrower focus on signal processing, including spectral analyses, and event detection and classification (e.g., Lesage, 2009; Messina and Langer, 2011; Bueno et al., 2020; Cortés et al., 2021). Finally, other software packages were developed to specifically perform seismic array data analyses (e.g., Pignatelli et al., 2008; Smith and Bean, 2020).

Here, we present MISARA (Matlab Interface for the Seismo-Acoustic aRary Analysis), a Matlab GUI that supports visualisation, detection and localization of volcano seismic and acoustic signals, with a focus on array techniques. In this manuscript, we will introduce the main features and functionalities of MISARA. We will demonstrate its use with two case studies to showcase the capabilities of the software in analysing volcano seismic waveforms, and discuss its suitability for both research and monitoring purposes.

OVERVIEW OF MISARA

MISARA is an open-source Matlab Interface that was developed to support users with the application of array techniques to seismic and acoustic signals. It is characterised by an intuitive and modular structure. MISARA is organised into different classes and modules, and its functionalities are accessed through a number of GUI windows (Fig. 1).

Home window

The Home window (Fig. 2) is the control panel of MISARA, which allows to manage all aspects of data processing, including data source configuration, Input/Output options and the parametrization of all analyses that can be performed on the selected data. The Home panel includes four dynamic menus to independently manage saving and importing the settings of the last analysis performed, or to load a suite of default analysis parameters. It allows access to all modules of MISARA, each dedicated to specific routines or algorithms for seismic and acoustic data processing.

Data preparation window

MISARA includes a module dedicated to the creation of appropriate data structures, that is the Create Dataset module (Fig. 3), which is accessed via the Data preparation window. MISARA works with seismic and acoustic waveforms archived, as Matlab structure arrays, in a dedicated folder/file structure. These files contain the raw data and some relevant metadata (e.g., station name, sampling rate, timing of records, etc.). MISARA modules require two additional files, which contain Matlab structures providing the station coordinates and information on the instrument response, respectively.

The software can operate in two modes, depending on whether the data source is an off-line archive or a web-based data server. In the off-line mode, the user can read and convert common file formats into MISARA structures; these formats include Seismic Analysis Code (SAC; Goldstein et al., 2003; Goldstein and Snoke, 2005), the Standard for the Exchange of Earthquake Data (SEED/miniSEED) and DSS-Cube/Data-Cube3 file format (see DATA AND RESOURCES). In the other mode, the user can access data stored at the Incorporated Research Institutions for Seismology-Data Management Center (IRIS-DMC) via International Federation of Digital Seismograph Networks (FDSN) services (see DATA AND RESOURCES), to retrieve waveforms and station/channel metadata. The off-line mode allows to recover information from XML files (eXtensible Markup Language). However, if the XML file are not available, it is possible to manually input station coordinates and instrument response parameters.

MISARA modules

All modules of MISARA share a similar design and workflow. All analysis parameters can be dynamically managed during data processing, including calculation, visualization and saving of the results (Fig. 4).

The Data Pre-processing modules (Fig. 1) are designed to perform data quality checks, and to deconvolve the instrument response from the raw seismograms as well as performed by other Matlab codes (e.g., Haney et al., 2012; Thompson and Reyes., 2018). In the case of seismic and acoustic array analyses, the Data Pre-processing modules also allow evaluation of the array response function by a Beam Pattern algorithm (Capon, 1969).

The Signal Features modules (Fig. 1) are based on well-established routines and algorithms used in seismic and acoustic signal processing, such as spectrograms (Schlindwein et al., 1995) and coherograms (Welch, 1967), Root Mean Square (RMS; Kenney and Keeping, 1962), polarization analysis (Jurkevics, 1988), Short Term Average/Long Term Average (STA/LTA; Allen, 1978) and the Sub-band Automatic LP Events Detection (SALPED; Garcia et al., 2017).

The Array modules (Fig. 1) implement the most used array processing algorithms for source localization of seismic and acoustic signals. This tool includes the Zero Lag Cross correlation analysis (ZLC; Frankel et al., 1991), MUltiple SIgnal Classification (MUSIC; Schmidt, 1986) algorithm, Semblance and Radial Semblance methods (Almendros et al., 2002). For the evaluation of the uncertainties in the estimate of the source position, we have implemented the JackKnife method (Efron, 1982). Additional details on all MISARA utilities are available in the help section of the software (https://doi.org/10.5281/zenodo.4642026).

EXAMPLES OF USE OF MISARA

We demonstrate the performances of MISARA through application to three cases studies, under different propagation models. First, we show the analysis of volcanic tremor recorded by a seismic array deployed at Mt. Etna (Italy) in 2011, when the volcano produced intense lava fountain activity from its New South East Crater (NSEC). Second, we demonstrate analyses of LP and VLP earthquakes recorded by Mt. Etna permanent seismic network in 2010, accompanying explosive activity at the Bocca Nuova crater (BN). Finally, we show the analysis the infrasound data acquired by an infrasound array deployed at Mt. Etna in 2019, when the NSEC crater was affected by intense Strombolian activity. Additional instructions on how to use of MISARA on these three case studies are available in the help section of the software by consulting the user manual and/or the video tutorials.

Case study 1: Mt. Etna, 2011-seismic array configuration

MISARA was tested using off-line data from a small-aperture seismic array in Etna volcano, Italy. The software configuration and its performances are summarized in Table A1. For this test, we used the Beam Pattern module to display the location of the array (Fig. 5a), its detailed geometry (Fig. 5b), and to evaluate its response function at a selected target frequency (Fig. 5c). The array consisted of five single-component seismometers with an aperture of approximately 200 m, deployed at a distance of about 1 km from NSEC. Figure 5c, suggests that the configuration of the array allows reliable array analyses in the frequency band 1 -3 .0 Hz, which coincides with the highest energy of volcanic tremor at Etna Volcano (e.g., Cannata et al., 2010). Indeed, the array showed a poor resolution at low frequency (0.5 Hz) because of the signal wavelength larger than the array aperture. Instead, it had a coherent response up to frequency of 3.0 Hz, while the influence of the spatial aliasing was more prevalent for increased frequencies.

The spectral energy and source location of volcanic tremor were retrieved by using the Spectrogram and ZLC modules, respectively. An example of analysis of volcanic tremor, recorded during the lava fountaining episode of 30 July, 2011 at NSEC, is shown in Figure 6. The results include time series of back-azimuth, ray parameter, tremor amplitude (RMS) and spectrogram linked to changes in eruptive activity. Significant variations in amplitude, frequency content and source location of tremor preceded and accompanied the onset of paroxysm, which corresponded to changes in the style and location of activity across different craters in the summit area of Mt. Etna (e.g., Patané et al., 2013; Moschella et al., 2018). Fig. 6a shows back-azimuths dominantly between -15°N and 5°N until about 7:00 am (UTC) on 30 July, pointing towards the NNE sector of Mt. Etna (Fig. 6f); between 7:00 and 8:00 am (UTC), which is twelve hours before the lava fountaining activity, the back-azimuth gradually migrated to 30-50°N (Fig. 6a), corresponding to arrivals from the NSEC direction (Fig. 6f).

Case study 2: Mt. Etna, 2010- seismic permanent network configuration

We also show the results of using MISARA with data from the permanent monitoring seismic network operated by the Istituto Nazionale di Geofisica e Vulcanologia (INGV). We used only signals recorded by seven stations deployed in the summit area of Mt. Etna (see Fig. 8 for station locations). These stations consisted of broadband three-component Trillium 40-s seismometers (Nanometrics^{TM}) recording at a sampling rate of 100 Hz. An overview of the configuration and performance of this second test is shown in Table A2. By using the STA/LTA and SALPED modules, we automatically detected LP and VLP events on the 23 October, 2010 (Fig. 7), when the BN crater produced moderate-to-intense Strombolian activity. We selected events on the basis of their features, such as frequency content (Fig. 7a), characteristic waveform (Fig. 7b) and particle motion of the signals (Fig. 7c).

Under the assumption of a homogeneous and isotropic propagation medium (waves velocity of 1.6 km/s), and thus of spherical wavefronts, we used the Semblance and Radial Semblance methods to track the source location of LP and VLP events, respectively. These two methods are similar to the backprojection one (Haney et al., 2014), that it is based on stacking of waveforms. However, unlike backprojection, Semblance returns the best performance for radial components of the wavefield, while Radial Semblance cannot be applied to non-radial components of the wavefield (Almendros et al., 2002). We employed a grid search approach by using only signals recorded by the seven INGV stations deployed in the summit area of Mt. Etna (see Fig. 8 for station locations). The results of this analysis are shown in Fig. 8. LP (Fig. 8a) and VLP (Fig. 8b) events were located below the BN crater at shallow depths, a common occurrence at Mt. Etna (e.g., Saccorotti et al., 2007; Cannata et al., 2009; Patanè et al., 2013; Zuccarello et al., 2013).

Case study 3: Mt. Etna, 2019- Infrasound array configuration

MISARA was also tested by using data from a small-aperture infrasound array in Etna volcano, Italy. These data have been already analysed in De Angelis et al. (2020), in which it is possible to retrieve additional information on the array and the results obtained by these authors. In particular, we focused on the infrasound signals recorded on 19th July, 2019, when the NSEC was affected by intense explosion activity. Trying to follow the same workflow, we configurated the software with the same parameters used in De Angelis et al. (2020). A brief summary on the parameters configuration and the analysis performances is shown in Table A3.

An example of analysis of these data by using MISARA is shown in Figure 9. In this case, we used Spectrogram and ZLC modules to determine the main features and the source position of infrasound signal, respectively. The results of the analysis in Figure 9 show that the software can reproduce those of De Angelis et al. (2020), especially in terms of amplitude, frequency content and source position of the infrasound signal. In particular, Fig. 9a shows back-azimuths focused on 60°N, pointing towards the NSEC (Fig. 9f), as well as the increase of the infrasound amplitude during the intensification of explosive activity (Figs. 9c,d, and e).

CONCLUSIONS

MISARA is a open-source Matlab-based GUI designed to perform analyses of seismic and acoustic waveform data. A suite of well-established algorithms for volcano seismic and acoustic signal processing have been integrated into our GUI interface, with a special focus on array techniques. We note that although MISARA was developed to facilitate the analysis of seismic and acoustic signals in volcanic environments, it can be used for other research purposes. Furthermore, owing to its modular structure (Fig. 1), it is possible to easily integrate additional functionalities.

The different data analysis modules of MISARA are independent of each other. The modules were designed to easily manage every step of the data processing and to quickly inspect the results (Fig. 4). Most of the processes are automated, reducing user's errors and efforts. One advantage consists of the possibility to reset some parameters directly from the module itself (Fig. 4), allowing to repeat the analysis many times. Other fundamental aspects of this modular structure are the possibility to deal with different formats of input traces, the systematic saving of the results and the optional activation of many subroutines (Fig. 4). In addition, most of the methods of source localization have implemented the JackKnife method, allowing an evaluation of the reliability of the results (e.g., Li et al, 2017; Moschella et al., 2018; Lehr et al., 2019, Sugimura et al., 2021).

The computational time for any type of analysis is crucially important, especially when there is the necessity to rapidly analyse real-time or quasi real-time recordings and/or a great amount of data. Although MISARA does not support real-time data processing, it may easily meet these requirements (e.g., Chao et al., 2017; Smith and Bean, 2020). By using a laptop with intermediate-high specifications (8 cores 2.90 GHz Intel(R) Core (TM) i7-10700 CPU, 16GB RAM), the processing times retrieved from the test cases (Tables A1 and A2; Fig. A1) are much shorter (a few seconds/minutes) than the duration of the analyzed time interval (1 day), speeding up the assessment of the parameters of interest and permitting in principle for real-time data analyses.

Successfully tested on the seismic data recorded during 2010-2011 period, the software demonstrates it suitability for different applications, such as academic/research uses, temporary surveys and operational purposes. Considering that tremor has long been considered as an important and reliable precursor of eruptive activity (e.g., McNutt et al., 2013; Zuccarello et al., 2013, 2022; Eibl et al., 2017), the results (Fig. 6) and the processing time (Table A1; Fig. A1) obtained for the analysis of volcanic tremor showed that seismic array data "have the potential to allow development of new strategies for early warning systems of eruptive activity at active volcanoes (e.g., Ripepe et al., 2018; Spina et al., 2020; Evita et al., 2021). The analysis of LP and VLP events has provided important information about the magma movement and the physical processes acting in the plumbing system of volcanoes (e.g., Chouet and Matoza, 2013 and references therein). Therefore, the analysis performed in the Case study 2 (Figs. 7 and 8) through MISARA modules could be useful to improve knowledge of the transport mechanisms of magma and eruption processes (e.g., Almendros et al., 2002; Zuccarello et al., 2013; Jousset et al., 2013; Giudicepietro et al., 2020; Sciotto et al., 2022). By reproducing the analysis shown in De Angelis et al. (2020), , methods included in MISARA are compatible with acoustic signal processing, as shown also in other recent works (e.g., McKee et al., 2017; Allstadt et al., 2018; Diaz-Moreno et al., 2020; De Angelis et al., 2021). In addition, thanks to the user-friendly and simple interface, MISARA could be suitable to quickly inspect seismo-acoustic traces during data collection.

Although MISARA has several advantages, it does not yet provide comprehensive solutions for all signal analyses. In addition, although most of MISARA processes are automated, some routines still include manual or semi-automatic phases. These features improve the data quality control and the robustness of the results compared to exclusively automatic ones, but they may sometimes represent an obstacle to fast analysis of the data.Pre-formatting routines in MISARA represent a possible alternative to the Python-based input and pre-processing procedures described in ObsPy (Beyreuther et al., 2010). In its current configuration, MISARA allows uploading data in a fast and clear manner, avoiding the repetition of any pre-processing routine in different modules of the software, or overloading the working memory. However, these routines could lead to duplication of data to the detriment of the storage space in contrast to ObsPy ones.

In order to improve the capabilities of MISARA toward a comprehensive assessment of volcano signals, future works should be aimed at: (*i*) simplifying the design and the structure of the software,providing an even more user-friendly GUI; (*ii*) implementing the existing algorithms by automating every phase of the data processing as much as possible (e.g., Álvarez et al., 2013; Bueno et al., 2019); (*iii*) adding further methods for more complete investigation of volcanic or seismological phenomena (e.g., De Barros et al., 2011; Zuccarello et al., 2016; Montesinos et al., 2021); (*iii*) adapting the GUI for real-time data processing and the exploitation of data streams provided by web services (e.g., Smith and Bean, 2020); (*iv*) integrating the GUI with well-established python libraries, such as ObsPy (Beyreuther et al., 2010), especially in terms of management of data and related metadata.

DATA AND RESOURCES

MISARA, its user's manual, and test/demonstration data can be downloaded at the URL: https://doi.org/10.5281/zenodo.4642026. The seismic and infrasound data used in this article were obtained from Istituto Nazionale di Geofisica e Vulcanologia, Osservatorio Etneo-Sezione di Catania (https://www.ct.ingv.it/). . The commercial platform, MATLAB, is from Mathworks, available at http://www.mathworks.com. A MATLAB script to download the Incorporated Research Institutions for Seismology (IRIS) seismic data archive can be found at https://ds.iris.edu/ds/nodes/dmc/manuals/irisfetchm/. For the management of the DSS-Cube/Data-Cube3 files, gipptools package is available at https://www.gfz-potsdam.de/en/section/geophysical-

imaging/infrastructure/geophysical-instrument-pool-potsdam-gipp/software/gipptools/.
Additional details on SAC and SEED formats are available at http://www.iris.edu/manuals/.

ACKNOWLEDGEMENTS

L. Zuccarello is supported by the project SINFONIA, progetto Bando Ricerca Libera 2021 Delibera 214/2021-INGV. S. De Angelis is supported by NERC grant NE/W004771/1. The authors thank the seismological technical staff of the Istituto Nazionale di Geofisica e Vulcanologia, Osservatorio Etneo-Sezione di Catania, , for their support in the acquisition of seismic data.

REFERENCES

- Aki K. and P. G. Richards (1980). Quantitative seismology, *WH Freeman*, San Francisco, doi: 10.1002/gj.3350160110.
- Allen, R. V. (1978). Automatic earthquake recognition and timing from single traces, *Bulletin of the seismological society of America*, 68(5), 1521-1532, doi: 10.1785/BSSA0680051521.
- Allstadt, K. E., R. S. Matoza, A. B. Lockhart, S. C. Moran, J. Caplan-Auerbach, M. M. Haney, A. T. Thelen and S. D. Malone (2018). Seismic and acoustic signatures of surficial

mass movements at volcanoes, *Journal of Volcanology and Geothermal Research,* 364, 76-106, doi: 10.1016/j.jvolgeores.2018.09.007.

- Almendros, J., B. Chouet, P. Dawson, and T. Bond (2002). Identifying elements of the plumbing system beneath Kilauea Volcano, Hawaii, from the source locations of very-long-period signals, *Geophysical Journal International*, 148(2), 303-312, doi: 10.1046/j.1365-246X.2002.01629.x.
- Almendros, J. and B. Chouet (2003). Performance of the radial semblance method for the location of very long period volcanic signals, *Bulletin of the Seismological Society of America,* 93(5), 1890-1903, doi: 10.1785/0120020143.
- Álvarez, I., L. García, S. Mota, G. Cortés, C. Benítez, and Á. De la Torre (2013). An automatic P-phase picking algorithm based on adaptive multiband processing, *IEEE Geoscience and remote sensing letters*, 10(6), 1488-1492, doi:10.1109/LGRS.2013.2260720.
- Beyreuther, M., R. Barsch, L. Krischer, T. Megies, Y. Behr, and J. Wassermann (2010). ObsPy: A Python toolbox for seismology, *Seismological Research Letters*, 81(3), 530-533, doi: 10.1785/gssrl.81.3.530.
- Bueno, A., C. Benitez, S. De Angelis, A. D. Moreno, and J. M. Ibáñez (2019). Volcano-seismic transfer learning and uncertainty quantification with Bayesian neural networks, *IEEE Transactions on Geoscience and Remote Sensing*, 58(2), 892-902. doi: 10.1109/TGRS.2019.2941494.

- Bueno, A., L. Zuccarello, A. D. Moreno, J. Woollam, M. Titos, C. Benítez, I. Álvarez, J. Prudencio and S. De Angelis (2020). PICOSS: Python interface for the classification of seismic signals, *Computers & geosciences*, 142, doi: 10.1016/j.cageo.2020.104531.
- Cannata, A., M. Hellweg, G. Di Grazia, S. Ford, S. Alparone, S. Gresta, P. Montalto and D. Patanè (2009). Long period and very long period events at Mt. Etna volcano: Characteristics, variability and causality, and implications for their sources, *Journal of Volcanology and Geothermal Research*, 187(3-4), 227-249, doi:10.1016/j.jvolgeores.2009.09.007.
- Cannata, A., G. Di Grazia, P. Montalto, F. Ferrari, G. Nunnari, D. Patanè, D., and E. Privitera (2010). New insights into banded tremor from the 2008–2009 Mount Etna eruption, *Journal of Geophysical Research: Solid Earth*, 115(B12), doi:10.1029/2009JB007120.
- Cannata, A., G. Di Grazia, M. Aliotta, C. Cassisi, P. Montalto, and D. Patanè (2013). Monitoring seismo-volcanic and infrasonic signals at volcanoes: Mt. Etna case study, *Pure and Applied Geophysics*, 170(11), 1751-1771, doi:10.1007/s00024-012-0634 x.
- Carbone, D., L. Zuccarello, and G. Saccorotti (2008). Geophysical indications of magma uprising at Mt Etna during the December 2005 to January 2006 non-eruptive period, *Geophysical Research Letters*, 35(6), doi: 10.1029/2008GL033212.
- Chao, W. A., Y. M. Wu, L. Zhao, H. Chen, Y. G. Chen, J. M. Chang, and C. M. Lin (2017). A first near real-time seismology-based landquake monitoring system, *Scientific reports*, 7(1), 1-12, doi: 10.1038/srep43510.

- Chouet, B. A., and R. S. Matoza (2013). A multi-decadal view of seismic methods for detecting precursors of magma movement and eruption, *Journal of Volcanology and Geothermal Research,* 252, 108-175, doi: 10.1016/j.jvolgeores.2012.11.013.

- Coombs, M. L., A. G. Wech, M. M. Haney, J. J. Lyons, D. J. Schneider, H. F. Schwaiger, K. L. Wallace, D. Fee, J. T. Freymueller, J. R. Schaefer, and G. Tepp (2018). Short-term forecasting and detection of explosions during the 2016–2017 eruption of Bogoslof volcano, Alaska, *Frontiers in Earth Science*, 6, 122, doi:10.3389/feart.2018.00122.

- Cortés, G., R. Carniel, P. Lesage, M. Á. Mendoza, and I. Della Lucia (2021). Practical volcano-independent recognition of seismic events: VULCAN. ears project, *Frontiers in Earth Science*, 8, 616676, doi:10.3389/feart.2020.616676.

- De Angelis, S., M. M. Haney, J. J. Lyons, A. Wech, D. Fee, A. Diaz-Moreno, and L. Zuccarello (2020). Uncertainty in detection of volcanic activity using infrasound arrays: examples from Mt. Etna, Italy, *Frontiers in Earth Science*, 8, 169, doi: 10.3389/feart.2020.00169.

- De Angelis, S., L. Zuccarello, S. Rapisarda and V. Minio (2021). Introduction to a community dataset from an infrasound array experiment at Mt. Etna, Italy, *Scientific Data*, 8(1), 1-9, doi: 10.1038/s41597-021-01030-6.

- De Barros, L., I. Lokmer, C. J. Bean, G. S. O'Brien, G. Saccorotti, J. P. Métaxian, L. Zuccarello, and D. Patanè (2011). Source mechanism of long-period events recorded by a high-density seismic network during the 2008 eruption on Mount Etna, *Journal of Geophysical Research: Solid Earth*, 116(B1), doi: 10.1029/2010JB007629.

- Diaz-Moreno, A., A. Roca, A. Lamur, B. H. Munkli, T. Ilanko, T. D. Pering, A. Pineda, and S. De Angelis (2020). Characterization of acoustic infrasound signals at Volcán de Fuego, Guatemala: a baseline for volcano monitoring, *Frontiers in Earth Science*, 8, 549774, doi: 10.3389/feart.2020.549774.
- Di Grazia, G., S. Falsaperla, and H. Langer (2006). Volcanic tremor location during the 2004 Mount Etna lava effusion, *Geophysical research letters*, 33(4), doi:10.1029/2005GL025177.
- Di Lieto, B., G. Saccorotti, L. Zuccarello, M. L. Rocca, and R. Scarpa (2007). Continuous tracking of volcanic tremor at Mount Etna, Italy, *Geophysical Journal International*, 169(2), 699-705, doi: 10.1111/j.1365-246X.2007.03316.x.
- Efron, B. (1982). The jackknife, the bootstrap and other resampling plans, *Society for industrial and applied mathematics*, doi: 10.1137/1.9781611970319.
- Eibl, E. P., C. J. Bean, K. S. Vogfjörd, Y. Ying, I. Lokmer, M. Möllhoff, G. S. O'Brien, and F. Pálsson (2017). Tremor-rich shallow dyke formation followed by silent magma flow at Bárðarbunga in Iceland, *Nature Geoscience*, 10(4), 299-304, doi:10.1038/ngeo2906.
- Euler, G. (2014). Project SEIZMO, Available at: http://epsc.wustl.edu/~ggeuler/codes/m/seizmo/.
- Evita, M., A. Zakiyyatuddin, S. Seno, N. S. Aminah, W. Srigutomo, I. Meilano, A. Setiawan, H. Darmawan, I. Suyanto, Irzaman, M. Yasin, Perdinan, R. Apsari, Wahyudi, W. Suryanto, and M. Djamal (2021). Development of Volcano Warning System for Kelud Volcano, *Journal of Engineering and Technological Sciences*, 53(2), 210202, doi: 10.5614/j.eng.technol.sci.2021.53.2.2.

- Frankel, A., S. Hough, P. Friberg, and R. Busby (1991). Observations of Loma Prieta aftershocks from a dense array in Sunnyvale, California, *Bulletin of the seismological Society of America*, 81(5), 1900-1922, doi: 10.1785/BSSA0810051900.
- Garcıa, L., I. Alvarez, M. Titos, A. D. Moreno, M. C. Benıtez, and A. de la Torre (2017). Automatic detection of long period events based on subband-envelope processing, *IEEE Journal of Selected Topics in Applied Earth Observations and Remote Sensing*, 10(11), 5134-5142, doi: 10.1109/jstars.2017.2739690.
- Giudicepietro, F., C. López, G. Macedonio, S. Alparone, F. Bianco, S. Calvari, W. De Cesare, D. Delle Donne, B. Di Lieto, A. M. Esposito, M. Orazi, R. Peluso, E. Privitera, P. Romano, G. Scarpato and A. Tramelli (2020). Geophysical precursors of the July-August 2019 paroxysmal eruptive phase and their implications for Stromboli volcano (Italy) monitoring, *Scientific reports*, 10(1), 1-16, doi: https://doi.org/10.1038/s41598-020-67220-1.
- Goldstein, P., D. Dodge, M. Firpo, L. Minner, W. Lee, H. Kanamori, P. Jennings, and C. Kisslinger (2003). SAC2000: Signal processing and analysis tools for seismologists and engineers, invited contribution to *The IASPEI International Handbook of Earthquake and Engineering Seismology*, Edited by WHK Lee, H. Kanamori, P.C. Jennings, and C. Kisslinger, Academic Press, London.
- Goldstein, P., and A. Snoke, (2005), SAC Availability for the IRIS Community, *Incorporated Research Institutions for Seismology Newsletter*, 7(UCRL-JRNL-211140), doi: https://www.osti.gov/servlets/purl/875360i

- Haney, M. M., J. Power, M. West, P. Michaels (2012). Causal Instrument Corrections for Short-Period and Broadband Seismometers, *Seismological Research Letters*; 83 (5): 834–845, doi: 10.1785/0220120031.
- Haney, M. M. (2014). Backprojection of volcanic tremor, *Geophysical Research Letters*, 41, 1923- 1928, doi:10.1002/2013GL058836.
- Havskov, J., and G. Alguacil (2016). Seismic Arrays, In *Instrumentation in Earthquake Seismology* (pp. 309-329), Springer, Cham, doi: 10.1007/978-3-319-21314-9_9.
- Inza, L. A., J. P. Métaxian, J. I. Mars, C. J. Bean, G. S. O'Brien, O. Macedo, and D. Zandomeneghi (2014). Analysis of dynamics of vulcanian activity of Ubinas volcano, using multicomponent seismic antennas, *Journal of Volcanology and Geothermal Research*, 270, 35-52., doi: 10.1016/j.jvolgeores.2013.11.008.
- Jousset, P., A. Budi-Santoso, A. D. Jolly, M. Boichu, Surono, S. Dwiyono, S. Dwiyono, S.Sumarti, S. Hidayati, and P. Thierry (2013). Signs of magma ascent in LP and VLP seismic events and link to degassing: an example from the 2010 explosive eruption at Merapi volcano, Indonesia, *Journal of Volcanology and Geothermal Research*, 261, 171-192, doi: 10.1016/j.jvolgeores.2013.03.014.
- Jurkevics, A. (1988). Polarization analysis of three-component array data, *Bulletin of the seismological society of America*, 78(5), 1725-1743, doi: 10.1785/BSSA0780051725.
- Kenney, J. F., and E. S. Keeping (1962). Root Mean Square, in *Mathematics of Statistics*, Pt. 1, 3rd ed. Princeton, NJ: Van Nostrand, pp. 59-60, 1962.

- Lehr, J., F. Eckel, M. Thorwart, W. and Rabbel (2019). Low-Frequency Seismicity at Villarrica Volcano: Source Location and Seismic Velocities, *Journal of Geophysical Research: Solid Earth*, 124(11), 11505-11530, doi: 10.1029/2018JB017023.
- Lesage, P. (2009). Interactive Matlab software for the analysis of seismic volcanic signals, *Computers & Geosciences*, 35(10), 2137-2144, doi: 10.1016/j.cageo.2009.01.010.
- Li, L., D. Becker, H. Chen, X. Wang, and D. Gajewski (2018). A systematic analysis of correlation-based seismic location methods, *Geophysical Journal International*, 212(1), 659-678, doi: 10.1093/gji/ggx436.
- McKee, K., D. Fee, A. Yokoo, R. S. Matoza, and K. Kim (2017). Analysis of gas jetting and fumarole acoustics at Aso Volcano, Japan, *Journal of Volcanology and Geothermal Research*, 340, 16-29, doi: 10.1016/j.jvolgeores.2017.03.029.
- McNutt, S. R., G. Thompson, M. E. West, D. Fee, S. Stihler, and E. Clark, (2013). Local seismic and infrasound observations of the 2009 explosive eruptions of Redoubt Volcano, Alaska, *Journal of Volcanology and Geothermal Research*, 259, 63-76., doi: 10.1016/j.jvolgeores.2013.03.016.
- McNutt, S. R., G. Thompson, J. Johnson, S. De Angelis, and D. Fee (2015). Seismic and infrasonic monitoring, In *The encyclopedia of volcanoes* (pp. 1071-1099), Academic Press., doi: 10.1016/B978-0-12-385938-9.00063-8.
- Messina, A., and H. Langer (2011). Pattern recognition of volcanic tremor data on Mt. Etna (Italy) with KKAnalysis—A software program for unsupervised classification, *Computers & Geosciences*, 37(7), 953-961, doi: 10.1016/j.cageo.2011.03.015.

- Montesinos, B. M., C. J. Bean, and I. Lokmer (2021). Quantifying strong seismic propagation effects in the upper volcanic edifice using sensitivity kernels, *Earth and Planetary Science Letters*, 554, doi: 10.1016/j.epsl.2020.116683.
- Morioka, H., H. Kumagai, and T. Maeda (2017). Theoretical basis of the amplitude source location method for volcano-seismic signals, *Journal of Geophysical Research: Solid Earth*, 122(8), 6538-6551, doi:10.1002/2017JB013997.
- Moschella, S., A. Cannata, G. Di Grazia, and S. Gresta (2018). Insights into lava fountain eruptions at Mt. Etna by improved source location of the volcanic tremor, *Annals of Geophysics*, doi: 10.4401/ag-7552.
- Patanè, D., A. Aiuppa, M. Aloisi, B. Behncke, A. Cannata, M. Coltelli, G. Di Grazia, S. Gambino, S. Gurrieri, M. Mattia, and G. Salerno (2013). Insights into magma and fluid transfer at Mount Etna by a multiparametric approach: A model of the events leading to the 2011 eruptive cycle, *Journal of Geophysical Research: Solid Earth*, 118(7), 3519-3539, doi: 10.1002/jgrb.50248.
- Pignatelli, A., A. Giuntini, and R. Console (2008). Matlab software for the analysis of seismic waves recorded by three-element arrays, *Computers & geosciences*, 34(7), 792-801, doi: 10.1016/j.cageo.2007.10.003.
- Ripepe, M., E. Marchetti, D. Delle Donne, R. Genco, L. Innocenti, G. Lacanna, and S. Valade (2018). Infrasonic early warning system for explosive eruptions, *Journal of Geophysical Research: Solid Earth*, 123(11), 9570-9585, doi: 10.1029/2018JB015561.

- Saccorotti, G., I. Lokmer, C. J. Bean, G. Di Grazia, and D. Patanè (2007). Analysis of sustained long-period activity at Etna Volcano, Italy, *Journal of volcanology and geothermal research*, 160(3-4), 340-354, doi: 10.1016/j.jvolgeores.2006.10.008.
- Schlindwein, V., J. Wassermann, and F. Scherbaum (1995). Spectral analysis of harmonic tremor signals at Mt. Semeru volcano, Indonesia, *Geophysical research letters*, 22(13), 1685-1688, doi: 10.1029/95GL01433.
- Schmidt, R. O. (1986). Multiple emitter location and signal parameter estimation, *IEEE Transactions on Antennas and Propagation*, 34, 276–280, doi: 10.1109/TAP.1986.1143830.
- Sciotto, M., A. Cannata, G. Di Grazia, and P. Montalto (2022). Volcanic tremor and long period events at Mt. Etna: Same mechanism at different rates or not?, *Physics of the Earth and Planetary Interiors*, 324, 106850, doi: 10.1016/j.pepi.2022.106850.
- Smith, P. J., and C. J. Bean (2020). RETREAT: A REal-Time TREmor Analysis Tool for Seismic Arrays, With Applications for Volcano Monitoring, *Frontiers in Earth Science*, 8, doi: 10.3389/feart.2020.586955.
- Sparks, R. S. J., J. Biggs, and J. W. Neuberg (2012). Monitoring volcanoes, *Science*, 335(6074), 1310-1311, doi:10.1126/science.1219485.
- Spina, R., A. Fornaia, and E. Tramontana (2020). VSEW: an early warning system for volcanic and seismic events, In *2020 IEEE International Conference on Smart Computing* (*SMARTCOMP*), 398-403, doi: 10.1109/SMARTCOMP50058.2020.00084.

- Sugimura, S., T. Nishimura, G. Lacanna, D. Legrand, S. Valade, and M. Ripepe (2021). Seismic Source Migration During Strombolian Eruptions Inferred by Very-Near-Field Broadband Seismic Network, *Journal of Geophysical Research: Solid Earth*, 126(12), doi: 10.1029/2021JB022623.
- Thompson, G., and C. Reyes (2018). GISMO-A Seismic Data Analysis Toolbox for MATLAB [software package], available at http:// geoscience community codes.github.io/GISMO/.
- Welch, P. (1967). The use of fast Fourier transform for the estimation of power spectra: a method based on time averaging over short, modified periodograms, *IEEE Transactions on audio and electroacoustics*, 15(2), 70-73, doi: 10.1109/TAU.1967.1161901.
- Zuccarello, L., M. R. Burton, G. Saccorotti, C. J. Bean, and D. Patanè (2013). The coupling between very long period seismic events, volcanic tremor, and degassing rates at Mount Etna volcano, *Journal of Geophysical Research: Solid Earth*, 118(9), 4910-4921, doi: 10.1002/jgrb.50363.
- Zuccarello, L., M. Paratore, M. La Rocca, F. Ferrari, A. Messina, S. Branca, D. Contrafatto, D. Galluzzo and S. Rapisarda (2016). Shallow velocity model in the area of Pozzo Pitarrone, Mt. Etna, from single station, array methods and borehole data, *Annals of Geophysics*, doi: 10.4401/ag-7086.

Zuccarello, L., S. De Angelis, V. Minio, G. Saccorotti, C. J. Bean, M. Paratore, and J. Ibáñez (2022). Volcanic tremor tracks changes in multi-vent activity at MountEtna, Italy: Evidence from analyses of seismic array data, *Geophysical Research Letters*, 49, e2022GL100056, doi: 10.1029/2022GL100056.

FULL MAILING ADDRESS FOR EACH AUTHOR

Minio Vittorio- vittorio.minio@phd.unict.it

Zuccarello Luciano-, luciano.zuccarello@ingv.it

De Angelis Silvio- silvioda@liverpool.ac.uk

Di Grazia Giuseppe- giuseppe.digrazia@ingv.it

Saccorotti Gilberto- gilberto.saccorotti@ingv.it

LIST OF FIGURE CAPTIONS

Figure 1. Schematic overview of MISARA. a) Data preparation window, for formatting the Input data. b) Home window, the main panel for the management of all the utilities of MISARA. c) Data Pre-processing modules, for the data quality control. d) Signal features modules, for those routines that support the array techniques, such as spectral, amplitude, polarization and detection analysis. e) Array analysis modules, for the source localization methods based on the multichannel techniques.

Figure 2. Example screenshot of the Home window, showing some of the configurable input parameters, the buttons for their management and the buttons to access to modules used for data formatting or analysis.

Figure 3. Example screenshot of Create Dataset module, showing the configurable parameters for the conversion of the Input files, the creation of the main data structures of the software and to retrieve waveforms and channel metadata.

Figure 4. Example of generic structure of MISARA modules. a) Axes figure, showing the main results. b) Reading files buttons, for the reading of the seismo-acoustic traces. c) Supplementary routines, for the management of additional analysis (for example, the calculation of the analysis error, the selection of the output results, the type of picking, etc…). d) Setting temporary parameters, for the management of those parameters that affects the analysis and the graphic elements. e) Command buttons, to control any process in the module, such as the calculation and visualization of the results, the saving of the Output data and figures and the calculation and visualization of secondary results. f) Text window, showing any information about the data processing through error, warning or command messages.

Figure 5. Examples of Output from Beam Pattern module by using a seismic array deployed at Mt. Etna during 2011. a) Array location (red triangle) on the Digital Elevation Model of the Eastern Sicily. b) Station locations showing the five-sensor array geometry with 200 m aperture, with vertical component Lennartz LE-3D/20s seismometers. c) Array response functions at 0.5, 1.0, 2.0, 3.0, 4.0 and 5.0 Hz; the colorbar on the right-hand side refers to the values of the Beam Pattern function.

Figure 6. Examples of output from Signal viewer, Spectrogram and ZLC modules by analysing volcanic tremor recorded on 30th July 2011. a) Temporal histogram of back-azimuth. It ranges between -15°N and 5°N, during quiescent periods of volcano activity, and between 30°N and 50°N, during eruptive activity. b) Temporal histogram of ray parameter. It increases with the onset

of eruptive activity from 0.6-1.0 s/km to 0.7-1.2 s/km, thus indicating a shallowing of the source. In (a) and (b), the results refer to the 1.0-1.5 Hz analysis range and they are filtered for cross correlation coefficients greater than 0.75; the colorbars on the right-hand side refer to the histogram probability. c) 1-hour long moving average of RMS amplitudes in 1.0-1.5 Hz frequency range at central station of the array. d) Seismic signal at the central station of the array. e) Spectrogram at the central station of the array; the colorbar indicates the power spectral density of the signal (PSD). f) Polar histogram of back-azimuth shown in (a) and plotted on the Digital Elevation Model of the summit area of Mt. Etna with the main craters (white circles; Bocca Nuova: BN; Voragine: VOR; North-East Crater: NEC; South-East Crater: SEC; New South-East Crater: NSEC). g) Bi-variate distribution (2D histogram) of ray parameter and back-azimuth shown in (a) and (b), respectively; the colorbar on the right-hand side refers to the histogram probability. Figure 7. Examples of output from SALPED and STA/LTA modules by analysing LP and VLP events recorded on 23rd October 2010 at ECPN station. a) Spectrograms of the LP and VLP events; most of the seismic radiation is focused around 1 and 0.05 Hz, respectively; the colorbar on the right-side refers to the normalized values of the spectral amplitude. b) Waveforms of LP/VLP events expressed in displacement. c) Particle motion of LP/VLP families on the summit portion of the Digital Elevation Model of Mt. Etna. In the analysis shown in (a), (b) and (c), the LP and VLP events were filtered between 0.5-1.2 Hz and 0.01-0.15 Hz, respectively.

Figure 8. Examples of output from Semblance and Radial Semblance modules by analysing LP and VLP events recorded on 23rd October 2010. Three sections of (a) Semblance and (b) Radial Semblance grids passing through the largest value node; the results represent the average distributions calculated on 38 LPs (a) and 51 VLP (b), respectively; the grid of 5x5x2 km^3 (E-W, N-S and vertical directions) is interpolated to the Digital Elevation Model of Mt. Etna; the

colorbars on the right-hand side refer to the normalized values of the Semblance/Radial Semblance.

Figure 9. Examples of output from Signal viewer, Spectrogram and ZLC modules by analysing infrasound signal recorded on 19th July 2019. a) Temporal histogram of back-azimuth. It ranges between 50N and 65°N during. b) Temporal histogram of ray parameter. The values range around 3 s/km. In (a) and (b), the results refer to the 0.7-15.0 Hz analysis range and they are filtered for cross correlation coefficients greater than 0.75; the colorbars on the right-hand side refer to the histogram probability. c) 1-hour long moving average of RMS amplitudes in 0.7-15.0 Hz frequency range at central station of the array. d) Infrasound signal at the central station of the array. e) Spectrogram at the central station of the array; the colorbar indicates the power spectral density of the signal (PSD). f) Polar histogram of back-azimuth shown in (a) and plotted on the Digital Elevation Model of the summit area of Mt. Etna with the main craters (white circles; Bocca Nuova: BN; Voragine: VOR; North-East Crater: NEC; South-East Crater: SEC; New South-East Crater: NSEC). g) Bi-variate distribution (2D histogram) of ray parameter and back-azimuth shown in (a) and (b), respectively; the colorbar on the right-hand side refers to the histogram probability.

Figure A1. Performance of the results showed in the sections Case study 1, Case study 2 and Case study 3. Each bar refers to the overall time required to perform the analyses summarised in the Tables A1, A2 and A3. The legend to the right-hand side of the diagram refers to the types of routines/subroutines activated during the processing of the data. This diagram does not take into account the differences in terms of the setting of input parameters or waveform data given in the Tables A1, A2 and A3.

FIGURES

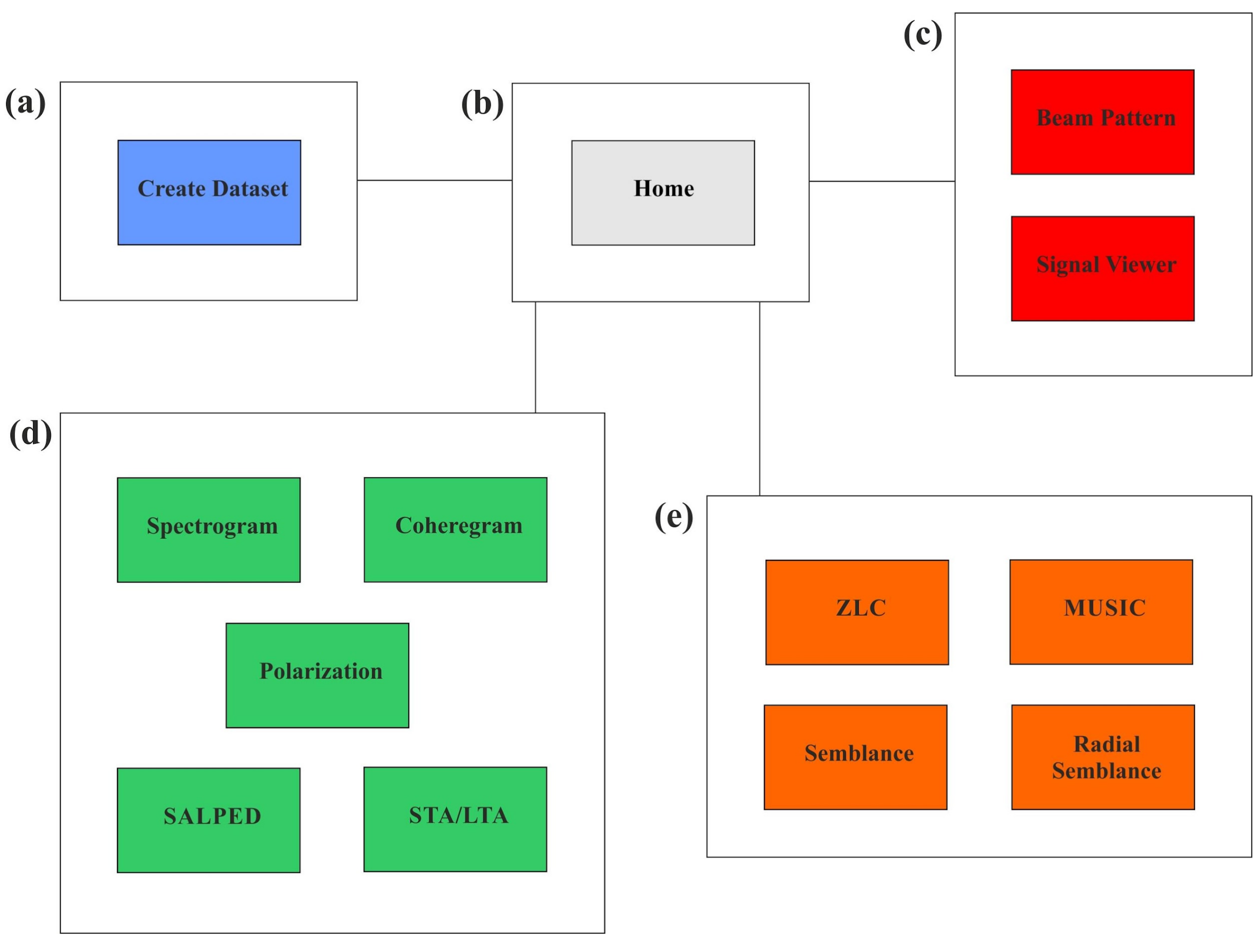

Figure 1. Schematic overview of MISARA. a) Data preparation window, for formatting the Input data. b) Home window, the main panel for the management of all the utilities of MISARA. c) Data Pre-processing, for the data quality control. d) Signal features modules, for those routines that

support the array techniques, such as spectral, amplitude, polarization and detection analysis. e) Array analysis modules, for the source localization methods based on the multichannel techniques.

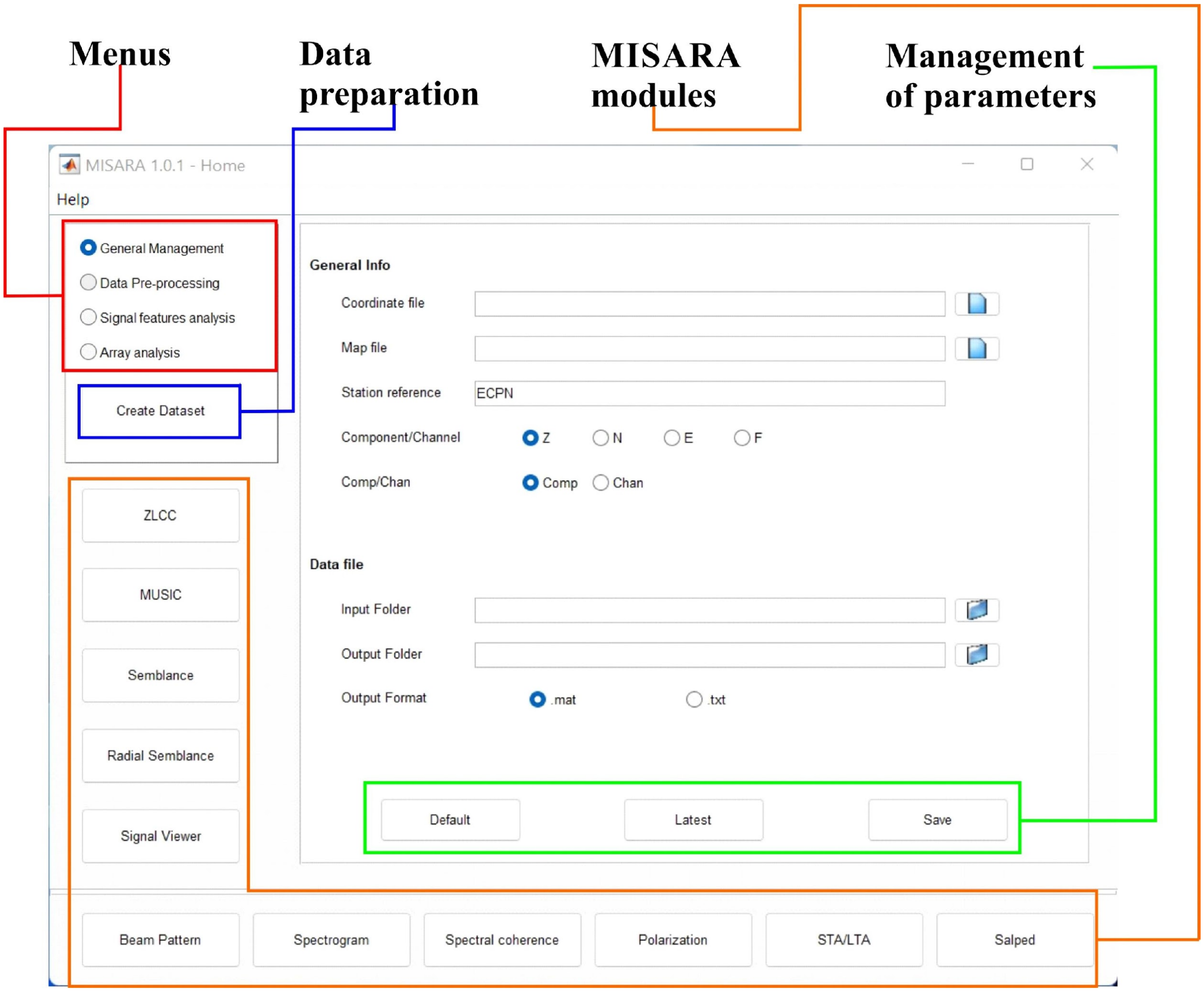

Figure 2. Example screenshot of the Home window, showing some of the configurable input parameters, the buttons for their management and the buttons to access to modules used for data formatting or analysis.

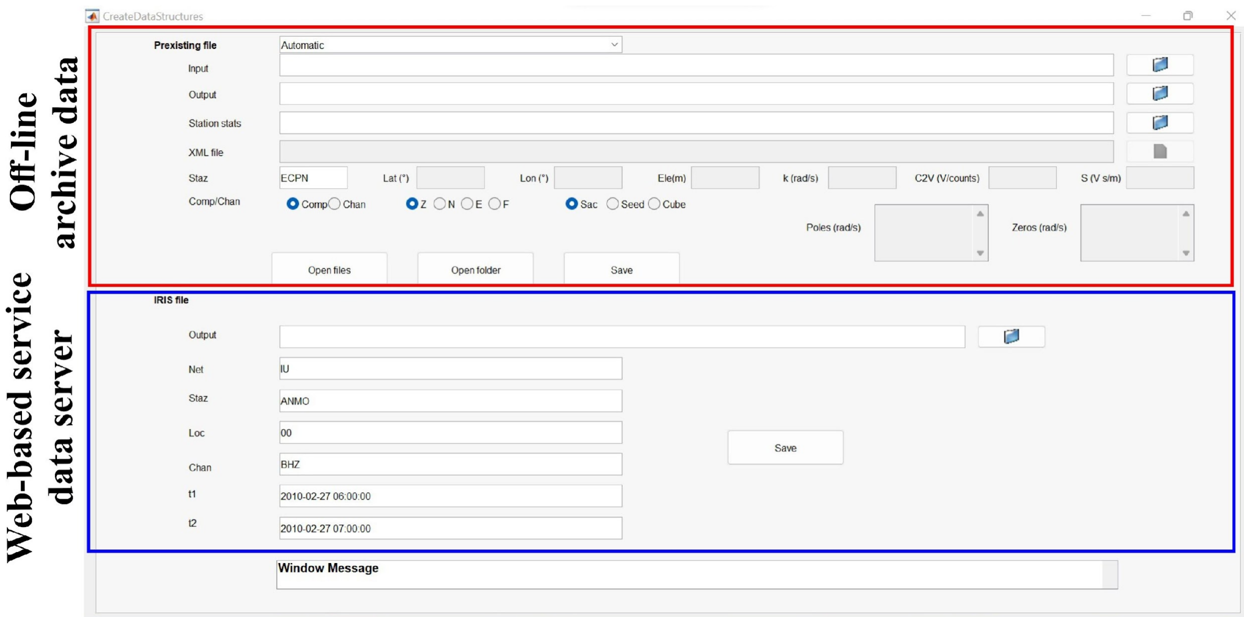

Figure 3. Example screenshot of Create Dataset module, showing the configurable parameters for the conversion of the Input files, the creation of the main data structures of the software and to retrieve waveforms and channel metadata.

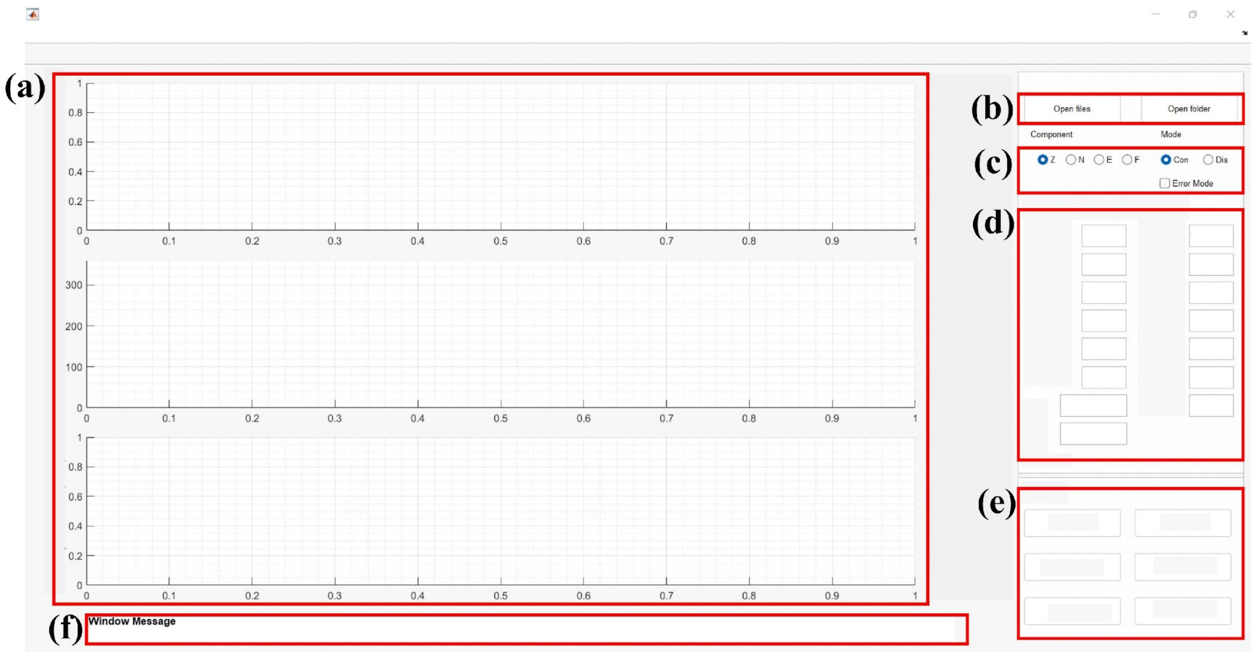

Figure 4. Example of generic structure of MISARA modules. a) Axes figure, showing the main results. b) Reading files buttons, for the reading of the seismo-acoustic traces. c) Supplementary routines, for the management of additional analysis (for example, the calculation of the analysis error, the selection of the output results, the type of picking, etc…). d) Setting temporary parameters, for the management of those parameters that affects the analysis and the graphic elements. e) Command buttons, to control any process in the module, such as the calculation and visualization of the results, the saving of the Output data and figures and the calculation and visualization of secondary results. f) Text window, showing any information about the data processing through error, warning or command messages.

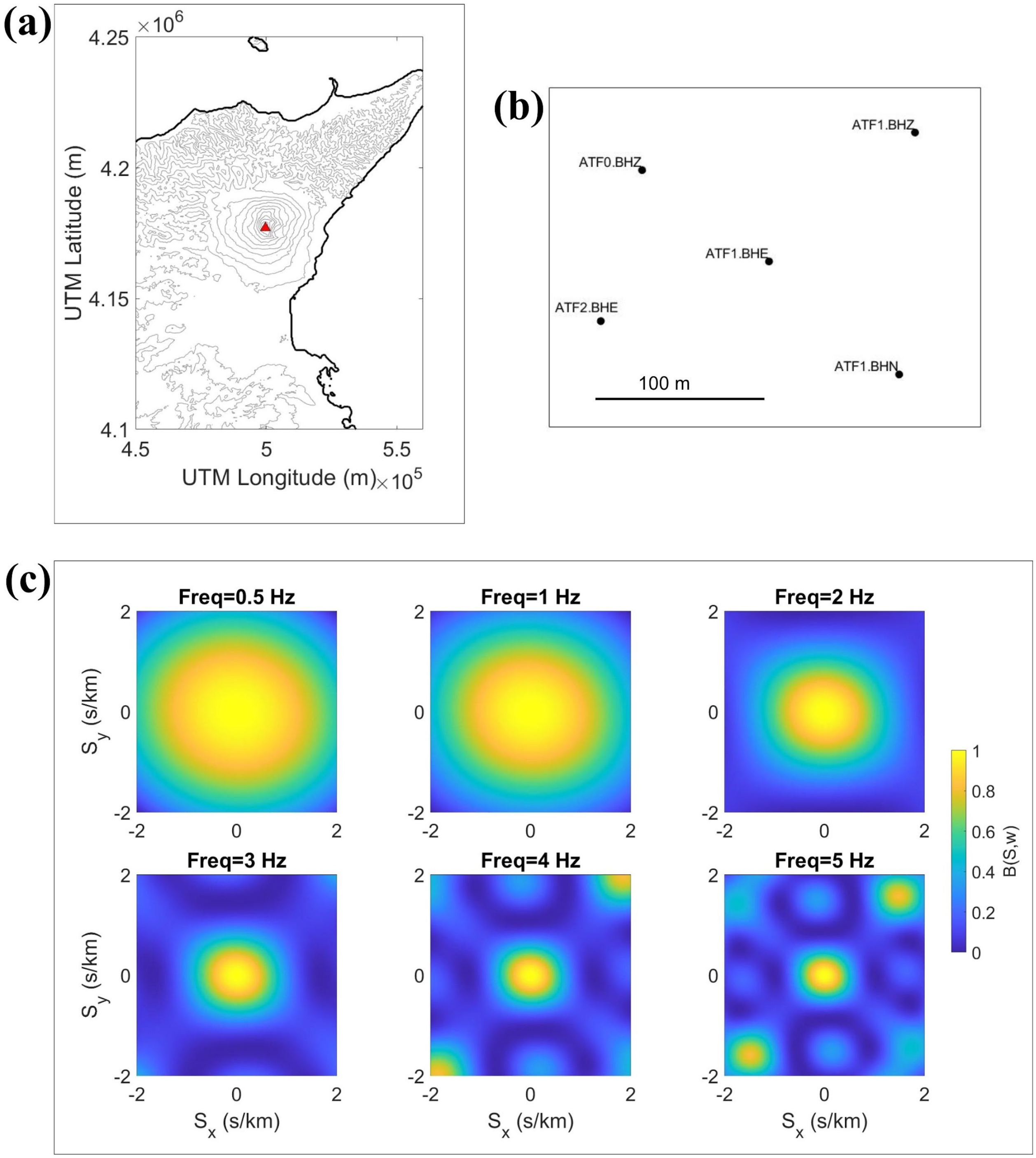

Figure 5. Examples of Output from Beam Pattern module by using a seismic array deployed at Mt. Etna during 2011. a) Array location (red triangle) on the Digital Elevation Model of the Eastern Sicily. b) Station locations showing the five-sensor array geometry with 200 m aperture, with vertical component Lennartz LE-3D/20s seismometers. c) Array response functions at 0.5, 1.0,

2.0, 3.0, 4.0 and 5.0 Hz; the colorbar on the right-hand side refers to the values of the Beam Pattern function.

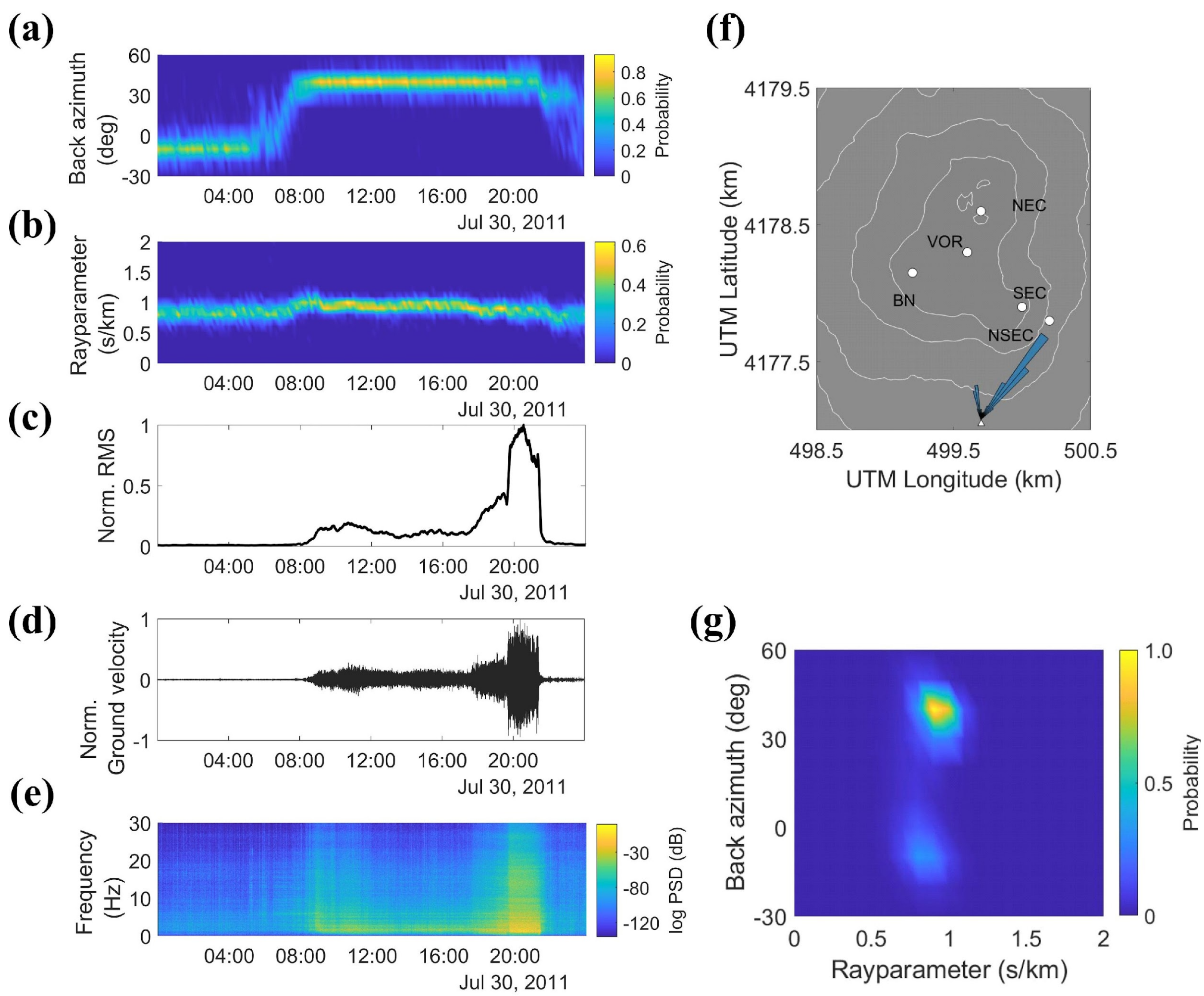

Figure 6. Examples of output from Signal viewer, Spectrogram and ZLC modules by analysing volcanic tremor recorded on 30th July 2011. a) Temporal histogram of back-azimuth. It ranges between -15°N and 5°N, during quiescent periods of volcano activity, and between 30°N and 50°N, during eruptive activity. b) Temporal histogram of ray parameter. It increases with the onset of eruptive activity from 0.6-1.0 s/km to 0.7-1.2 s/km, thus indicating a shallowing of the source.

In (a) and (b), the results refer to the 1.0-1.5 Hz analysis range and they are filtered for cross correlation coefficients greater than 0.75; the colorbars on the right-hand side refer to the histogram probability. c) 1-hour long moving average of RMS amplitudes in 1.0-1.5 Hz frequency range at central station of the array. d) Seismic signal at the central station of the array. e) Spectrogram at the central station of the array; the colorbar indicates the power spectral density of the signal (PSD). f) Polar histogram of back-azimuth shown in (a) and plotted on the Digital Elevation Model of the summit area of Mt. Etna with the main craters (white circles; Bocca Nuova: BN; Voragine: VOR; North-East Crater: NEC; South-East Crater: SEC; New South-East Crater: NSEC). g) Bi-variate distribution (2D histogram) of ray parameter and back-azimuth shown in (a) and (b), respectively; the colorbar on the right-hand side refers to the histogram probability.

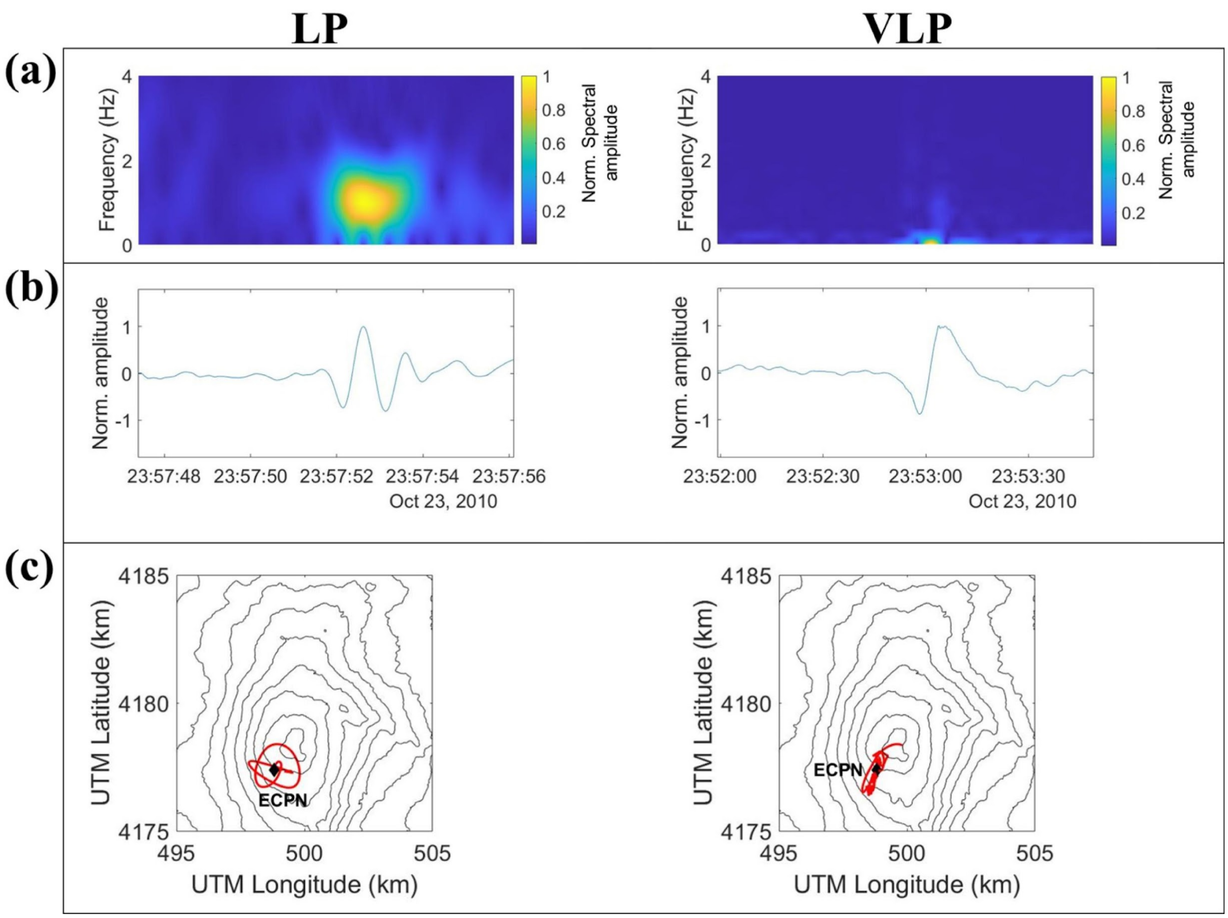

Figure 7. Examples of output from SALPED and STA/LTA modules by analysing LP and VLP events recorded on 23rd October 2010 at ECPN station. a) Spectrograms of the LP and VLP events; most of the seismic radiation is focused around 1 and 0.05 Hz, respectively; the colorbar on the right-side refers to the normalized values of the spectral amplitude. b) Waveforms of LP/VLP events expressed in displacement. c) Particle motion of LP/VLP families on the summit portion of the Digital Elevation Model of Mt. Etna. In the analysis shown in (a), (b) and (c), the LP and VLP events were filtered between 0.5-1.2 Hz and 0.01-0.15 Hz, respectively.

LP

(a)

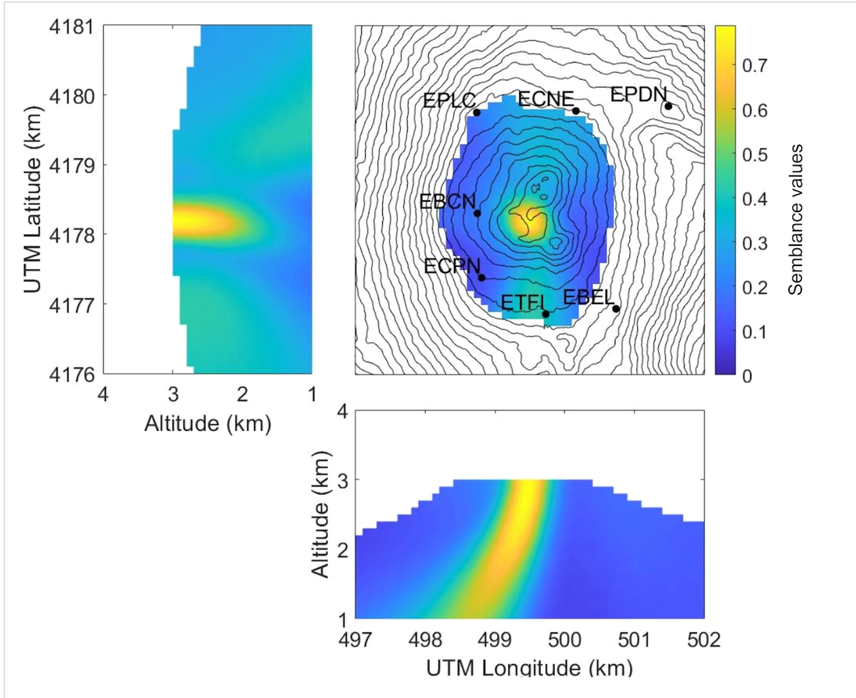
4181
4180
4179
4178
4177
4176
UTM Latitude (km)
4
3
2
1
Altitude (km)
EPLC
ECNE
EPDN
EBCN
ECPN
ETFL
EBEL
0.7
0.6
0.5
0.4
0.3
0.2
0.1
0
Semblance values
Altitude (km)
497
498
499
500
501
502
UTM Longitude (km)

VLP

(b)

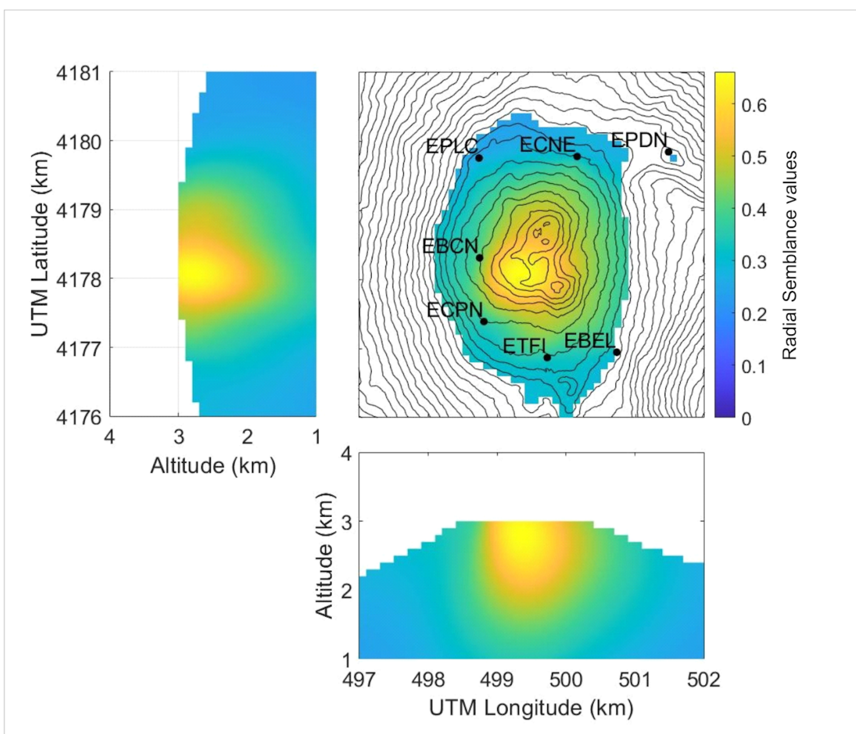
4181
4180
4179
4178
4177
4176
UTM Latitude (km)
4
3
2
1
Altitude (km)
EPLC
ECNE
EPDN
EBCN
ECPN
ETFL
EBEL
0.6
0.5
0.4
0.3
0.2
0.1
0
Radial Semblance values
Altitude (km)
497
498
499
500
501
502
UTM Longitude (km)

Figure 8. Examples of output from Semblance and Radial Semblance modules by analysing LP and VLP events recorded on 23rd October 2010. Three sections of (a) Semblance and (b) Radial Semblance grids passing through the largest value node; the results represent the average distributions calculated on 38 LPs (a) and 51 VLP (b), respectively; the grid of 5x5x2 km^3 (E-W, N-S and vertical directions) is interpolated to the Digital Elevation Model of Mt. Etna; the colorbars on the right-hand side refer to the normalized values of the Semblance/Radial Semblance.

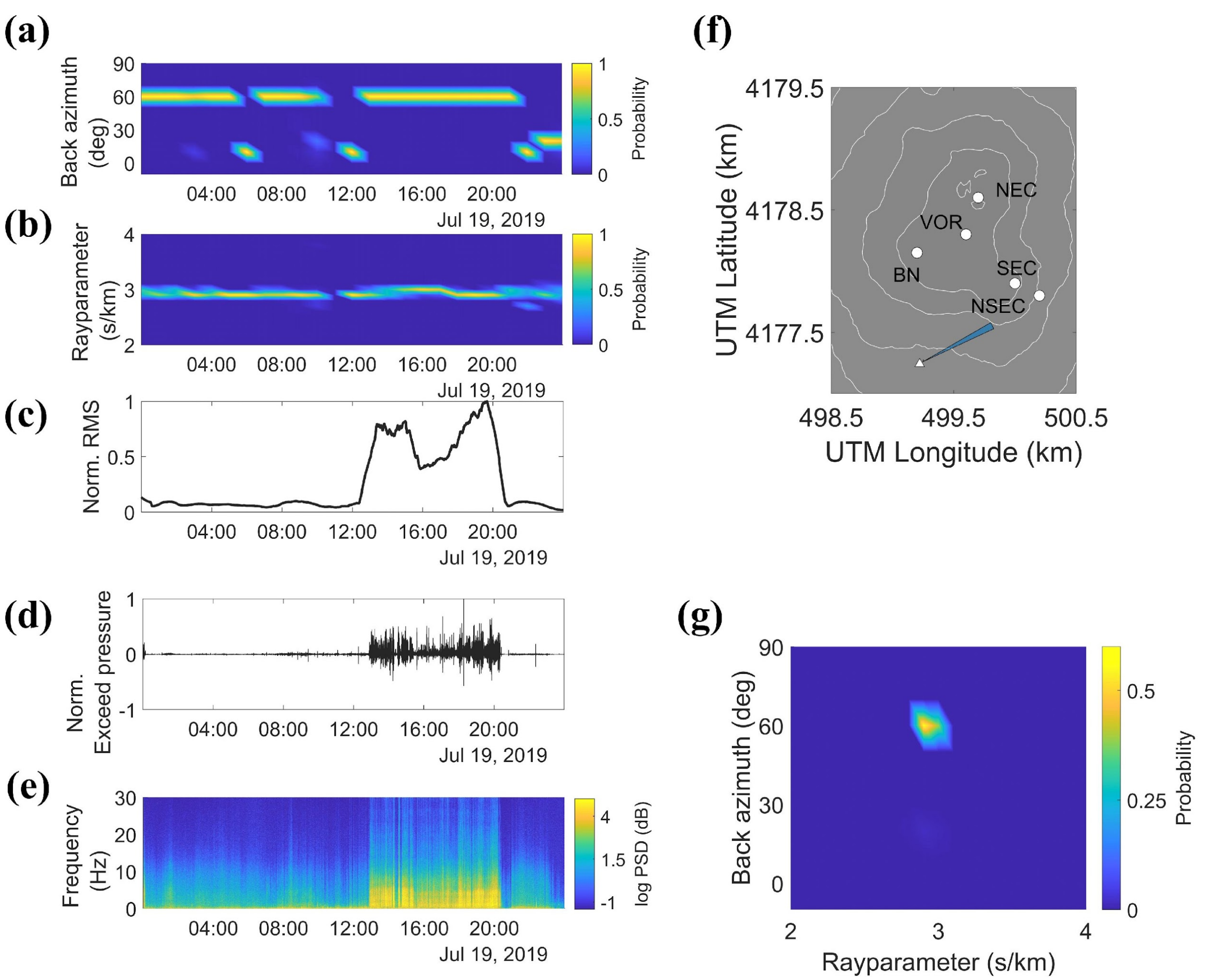

Figure 9. Examples of output from Signal viewer, Spectrogram and ZLC modules by analysing infrasound signal recorded on 19th July 2019. a) Temporal histogram of back-azimuth. It ranges between 50N and 65°N during. b) Temporal histogram of ray parameter. The values range around 3 s/km. In (a) and (b), the results refer to the 0.7-15.0 Hz analysis range and they are filtered for cross correlation coefficients greater than 0.75; the colorbars on the right-hand side refer to the histogram probability. c) 1-hour long moving average of RMS amplitudes in 0.7-15.0 Hz frequency range at central station of the array. d) Infrasound signal at the central station of the array. e) Spectrogram at the central station of the array; the colorbar indicates the power spectral density of the signal (PSD). f) Polar histogram of back-azimuth shown in (a) and plotted on the Digital Elevation Model of the summit area of Mt. Etna with the main craters (white circles; Bocca Nuova: BN; Voragine: VOR; North-East Crater: NEC; South-East Crater: SEC; New South-East Crater: NSEC). g) Bi-variate distribution (2D histogram) of ray parameter and back-azimuth shown in (a) and (b), respectively; the colorbar on the right-hand side refers to the histogram probability.

APPENDICES

Table A1. Summary of the analysis of volcanic tremor recorded on 30th July 2011 by using Beam Pattern, Spectrogram and ZLC modules.

Method	Settings	Waveform data	Output size	Timing
Beam Pattern	Frequency (Hz): 0.5-5.0 Frequency step (Hz): 0.5 Grid size (s^2/km^2): 2x2 Grid step (s/km): 0.05			Data processing (s): ~0.30

Spectrogram	Window (s): 60 N° samples spectra: 8192 High pass filter (Hz): 0.01 Averaging factor (min): 30	Sample rate (Hz): 100 Sample count: 8460000 N° sensors: 1 vertical component	~2.41 MB	Data processing (s): ~1.07 Data saving (s): ~0.52
RMS	Window (s): 10 Frequency band (Hz): 0.5-1.5 Averaging factor (min): 60	Sample rate (Hz): 100 Sample count: 8460000 N° sensors: 1 vertical component	~117 KB	Data processing (s): ~0.83 Data saving (s): ~0.15
ZLC	Window (s): 10 Frequency band (Hz): 0.5-1.5 Velocity waves (km/s): 1.6 km Max delay time (s): 4 Spline interpolation: True Histogram bin (min): 60 Correlation threshold: 0.75	Sample rate (Hz): 100 Sample count: 8460000 N° sensors: 5 vertical component	~579 KB	Data processing (s): ~23.83 Data processing with jackkinfe (s): ~88.09 Data saving (s): ~0.25

Table A2. Summary of the analysis of LP and VLP events recorded on 23rd October 2010 by using STA/LTA, SALPED, Semblance and Radial Semblance modules.

Method	Settings	Waveform data	Output size	Timing
STA/LTA	Frequency band (Hz): 0.01-0.15 STA window (s): 6 LTA window (s): 60 Detection threshold: 2.5 Window spectrogram (s): 5.28 Overlap window spectrogram (s): 5.20 N° samples spectra: 1024 Window polarization (s): 5	Sample rate (Hz): 100 Sample count: 8460000 N° sensors: 1 three components	~86.50 MB	Data processing (s): ~1.97 Spectral data processing (s): ~24.99 (~0.49 per event) Polarization data processing (s): ~19.38 (~0.38 per event) Data saving (s): ~51.29 (~1.01 per event)
SALPED	Central frequency brand (Hz): 0.5-1.2 Lower frequency band (Hz): 0.1-0.4 Upper frequency band (Hz): 3-10 Windows (s): ± 5 Detection threshold: 1.0 Window spectrogram (s): 1.28 Overlap window spectrogram (s): 1.20 N° samples spectra: 128 Window polarization (s): 2.5	Sample rate (Hz): 100 Sample count: 8460000 N° sensors: 1 three components	~11.70 MB	Data processing (s): ~2.24 Spectral data processing (s): ~17.10 (~0.45 per event) Polarization data processing (s): ~13.68 (~0.36 per event) Data saving (s): ~38.22 (~1.01 per event)

Semblance	Window (s): 2.5 Frequency band (Hz): 0.5-1.2 Central frequency (Hz): 1 Grid size (km^3): 5x5x2 Grid step (km): 0.1 Quality factor: 40 Velocity waves (km/s): 1.6 km Attenuation factor: 1	Sample rate (Hz): 100 Sample count: 1000 N° sensors: 7 three components N° events: 38	~12.10 MB	Data processing (s): ~28.72 (~0.75 per event) Data processing with jackkinfe (s): ~230 (~6.05 per event) Data saving (s): ~1.30
Radial Semblance	Window (s): 5 Frequency band (Hz): 0.01-0.15 Grid size (km^3): 5x5x2 Grid step (km): 0.1 Velocity waves (km/s): 1.6 km	Sample rate (Hz): 100 Sample count: 12000 N° sensors: 7 three components N° events: 51	~15. 30 MB	Data processing (s): ~211.76 (~4.15 per event) Data processing with jackkinfe (s): ~1 694.08 (~33.22 per event) Data saving (s): ~1.75

Table A3. Summary of the analysis of infrasound signal recorded on 19th July 2019 by using Spectrogram and ZLC modules.

Method	Settings	Waveform data	Output size	Timing
Spectrogram	Window (s): 60 N° samples spectra: 8192 High pass filter (Hz): 0.01 Averaging factor (min): 30	Sample rate (Hz): 100 Sample count: 8460000 N° sensors: 1 vertical component	~1.86 MB	Data processing (s): ~0.98 Data saving (s): ~0.37

RMS	Window (s): 10 Frequency band (Hz): 0.7-15 Averaging factor (min): 60	Sample rate (Hz): 100 Sample count: 8460000 N° sensors: 1 vertical component	~192 KB	Data processing (s): ~0.81 Data saving (s): ~0.35
ZLC	Window (s): 10 Frequency band (Hz): 0.7-15 Velocity waves (km/s): 0.354 km Max delay time (s): 4 Spline interpolation: True Histogram bin (min): 60 Correlation threshold: 0.75	Sample rate (Hz): 100 Sample count: 8460000 N° sensors: 6 vertical component	~460 KB	Data processing (s): ~24.01 Data processing with jackkinfe (s): ~87.54 Data saving (s): ~0.31

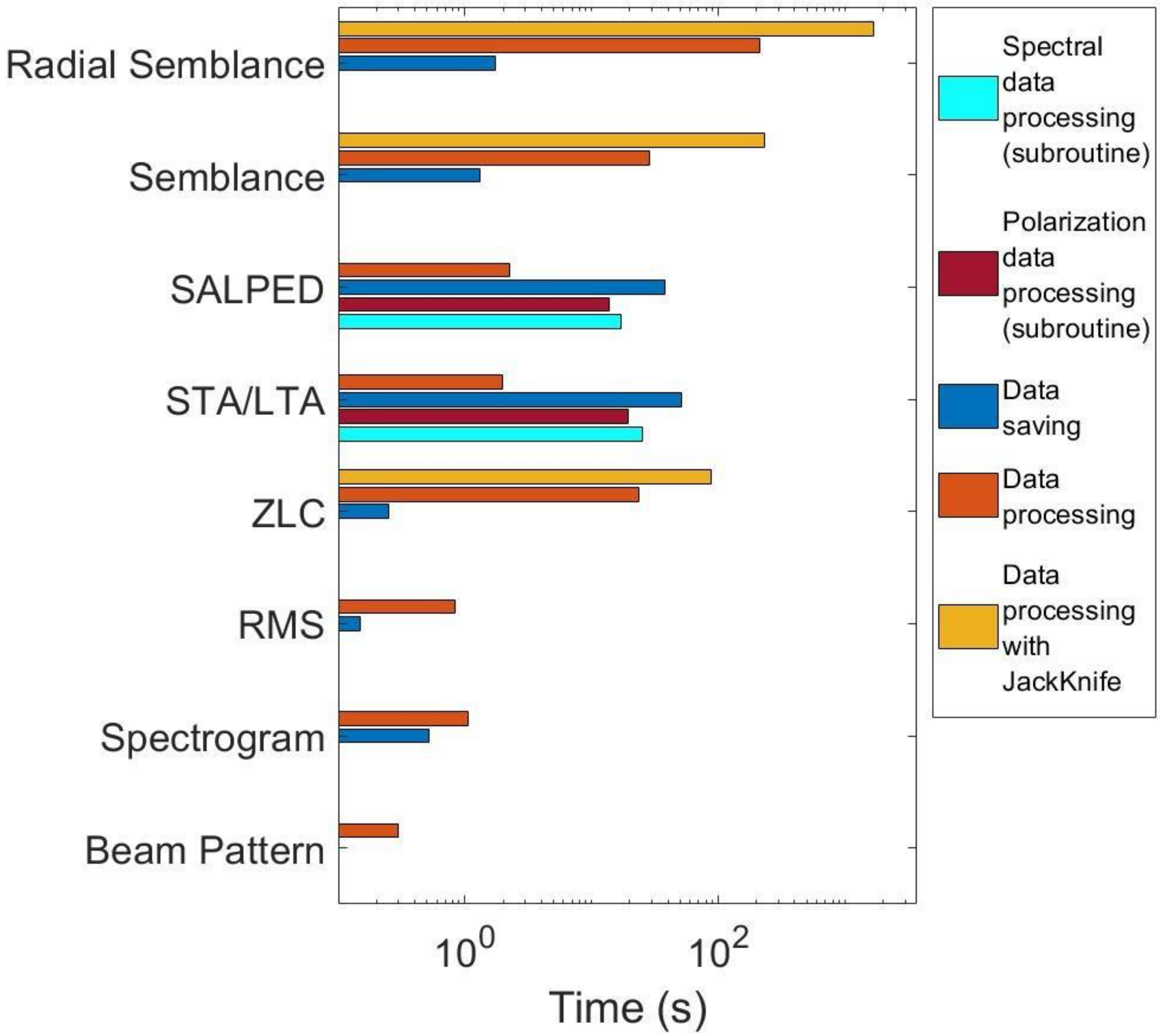

Figure A1. Performance of the results shown in the sections Test Case study 1, Case study 2 and Case study 3. Each bar refers to the overall time required to perform the analyses summarised in the Tables A1, A2 and A3. The legend to the right-hand side of the diagram refers to the types of routines/subroutines activated during the processing of the data. This diagram does not take into account the differences in terms of the setting of input parameters or waveform data given in the Tables A1, A2 and A3.